We are IntechOpen,
the world's leading publisher of
Open Access books
Built by scientists, for scientists

6,900
Open access books available

185,000
International authors and editors

200M
Downloads

Our authors are among the

154
Countries delivered to

TOP 1%
most cited scientists

12.2%
Contributors from top 500 universities

BOOK CITATION INDEX
CLARIVATE ANALYTICS
INDEXED

WEB OF SCIENCE™

Selection of our books indexed in the Book Citation Index
in Web of Science™ Core Collection (BKCI)

Interested in publishing with us?
Contact book.department@intechopen.com

2D Fourier Fractal Analysis of Optical Coherence Tomography Images of Basal Cell Carcinomas and Melanomas

Wei Gao, Bingjiang Lin, Valery P. Zakharov and Oleg O. Myakinin

Abstract

The optical coherence tomography (OCT) technique is applied in the diagnosis of the skin tissue. In general, quantitative imaging features obtained from OCT images have already been used as biomarkers to categorize skin tumors. Particularly, the fractal dimension (FD) could be capable of providing an efficient approach for analyzing OCT images of skin tumors. The 2D Fourier fractal analysis (FFA) as well as the differential box counting method (DBCM) was used in this paper to classify the basal cell carcinomas (BCC), melanomas, and benign melanocytic nevi. Generalized estimating equations were used to test for differences between skin tumors. Our results showed that the significant decrease of the 2D FD was detected in the benign melanocytic nevi and basal cell carcinomas as compared with the melanomas. Our results also suggested that the 2D FFA could provide a more efficient way to calculating FD to differentiate the basal cell carcinomas, melanomas, and benign melanocytic nevi as compared to the 2D DBCM.

Keywords: skin tumor, basal cell carcinomas, melanomas, fractal dimension, differential box counting method, Fourier fractal analysis, optical coherence tomography

1. Introduction

The OCT technique is an optical imaging modality that could provide high-resolution and cross-sectional visualization of biological tissues [1]. The OCT technique was firstly utilized for imaging retinal tissue [2]. In 1997, the OCT technique was used in the evaluation and the detection of diseases in the skin because it can detect the diseases or wounds in a noninvasive way. The burn wounds and the wound healing processes have been studied by using the OCT technique [3–5]. By utilizing the OCT technique, the morphological changes of skin tissue can be obtained from OCT images. Besides, the OCT technique has been used to analyze the differences in morphological changes in skin tumors [6]. Particularly, the morphological changes can be used as an indicator to characterize the different types of skin tumors.

An automatic texture analysis of OCT images did not have a long history. Gan et al. received accuracy of the atrial tissue disease definition in 80% for OCT imaging, using his own method with automatic detection of regions of interest [7]. Scientists from Stanford offered automatic classifier to determine the basal cell carcinomas by using polarization-sensitive OCT that could achieve the sensitivity and specificity of about 85% [8]. Lingley-Papadopoulos et al. used texture analysis for diseases of the bladder, receiving sensitivity of 92% and specificity of 62% [9]. Gambichler et al. in their work received a sensitivity of about 75% and a specificity of about 93% for the melanomas and nevi in the skin tissue [10]. Multi-beam OCT system has been successfully used to identify the basal cell carcinomas with the sensitivity of 96% and specificity of 75% [11]. The multimodal approach to the problem of separation of intestinal adenocarcinomas from healthy bowel tissue, using texture analysis of OCT images and chemical information Raman spectroscopy, gives the sensitivity and specificity of 94% [12]. Fourier analysis and texture analysis of OCT images of breast tissues ex vivo using Fisher's linear discriminate analysis gives the result as 100% sensitivity and specificity for the normal and pathology case and 90 and 85%, respectively, for the benign/malignant tumors case [13].

Based on the fact that the affected tissue is characterized by the distinct structural changes at the molecular, cellular, and tissue architecture levels, the fractal dimension performed by the fractal analysis can be used to analyze the disease-dependent irregularities in shape. In 1967, Mandelbrot firstly introduced the concept of the fractal dimension to describe the self-similar pattern when he measured the length of the coastline of the United Kingdom [14]. Mandelbrot found that the total length of the coastline changed when he used the different size of ruler to measure the length of coastline. Therefore, he employed the FD as a scale that was applied to the ruler. The scale can be recognized as an indicator to describe the roughness of a surface such as the coastline. And due to this description, the complexity of an object can be evaluated by using the FD. Higher values of the FD mean the higher roughness of the surfaces. Fractal analysis has already been used to study the morphological change of skin tumors.

Hussain et al. used the box counting method to find out the dimensions of the affected cells in skin tumors [15]. Karimi and Farshchi calculated the FD from micros by using the box counting method for differentiating normal moles (nevi) from melanomas [16]. Gao et al. used the 2D DBCM to extract the FD from OCT images for classifying the skin tumors [17]. In those studies, the box counting method (including the DBCM) was applied to the skin tumors' images for extracting the FD.

Though the box counting method is a reasonable methodology to calculate the FD from the skin tumors' images, it is a low-efficient and time-consuming methodology that counts the boxes for calculating FD. In order to improve the efficacy, it is necessary to employ a cheaper and more efficient methodology to extract FD from the images. In this paper, the 2D Fourier fractal methodology was used to reduce the computational time of FD from OCT images. The spectral domain OCT (SD-OCT) was used to collect images for the basal cell carcinomas, melanomas, and benign melanocytic nevi.

2. Methodology

2.1 OCT system and data collection

The SD-OCT equipment was assembled in the department of laser and biotechnical system at the Samara National Research University. The schematic diagram

is showed in **Figure 1**. The equipment was characterized by the 14 mW output power, 45 nm light source bandwidth, 840 nm central wavelength, and axial/lateral resolution ca. 6 μm. A Michelson interferometer in the equipment was used to split the incident light in a 50/50 ration for the sample and reference arms. A diffraction grating that could be capable for providing 1200 groves per millimeter and a CCD line scan camera that has the 29.3 kHz line rate in 4096 pixel resolution are assembled in the spectrometer. The image acquisition card for digitizing the signal is NI-IMAQ PCI-1428.

This study included three universities that are the Samara State Medical University, Samara National Research University, and Ningbo University of Technology. The institutional review board of each institution approved the study protocol. This research adhered to the tenets set forth in the Declaration of Helsinki. Informed consent of each subject was obtained.

2.2 OCT images and OCT image processing

The samples of skin tumor with the typical macroscopic features were selected from the surgical removal. Three types of skin tumors were included in this study, which are malignant melanoma, benign melanocytic nevus, and basal cell carcinoma (BCC).

The OCT image of the benign melanocytic nevus obtained by using the SD-OCT was showed in **Figure 2**. The structure of the epidermis in OCT images of benign melanocytic nevus was typical for a healthy skin, although it featured a certain amount of melanocytes and pigmented keratinocytes. As compared to benign melanocytic nevus, basal cell carcinoma and melanoma showed the signs of malignancy that could be used to differentiate themselves from benign melanocytic nevi and normal skin tissue. The OCT image of the basal cell carcinoma was showed in **Figure 3**. The image clearly indicated that the basal cell carcinoma tumor cells were roundish or elliptical in shape. In the periphery of the tumor mass, the basal cell carcinoma cells had palisading arrangement. The optical densities in basal cell carcinoma and normal skin tissue are different, in which the basal cell carcinoma in OCT images showed a darker color. The OCT image of the melanoma was showed in **Figure 4**. In the OCT image, the healthy epidermis can be seen as a bright band on the skin tissue's surface. The melanin complex and the small undifferentiated cells
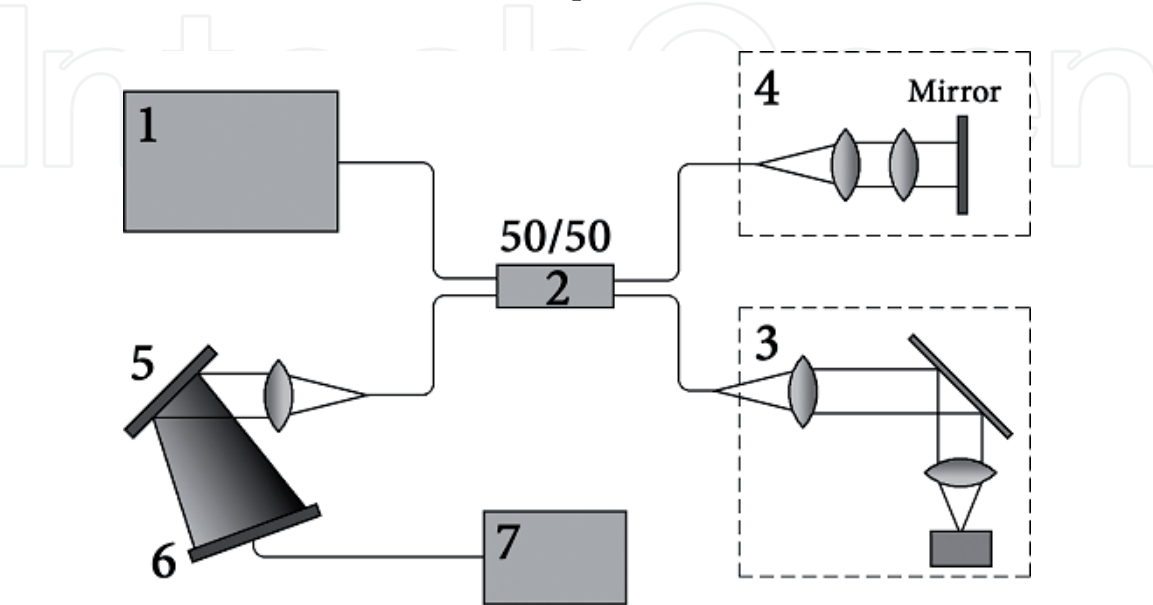

Figure 1.
The custom-built SD-OCT system. (1) Broadband light source, (2) 50/50 beam splitter, (3) sample arm, (4) reference arm, (5) spectrometer with grating, (6) CCD camera, and (7) computer with IMAQ.
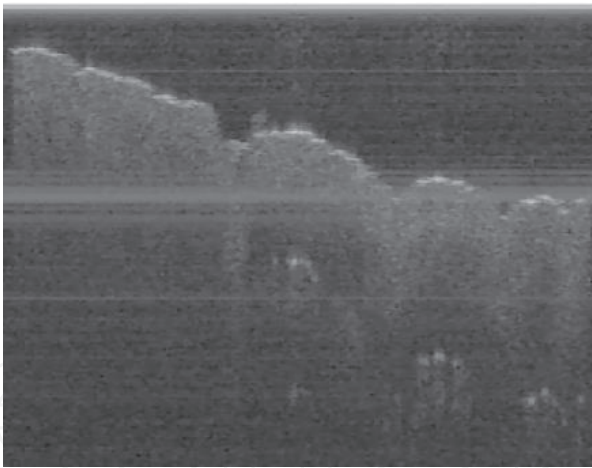
Figure 2.
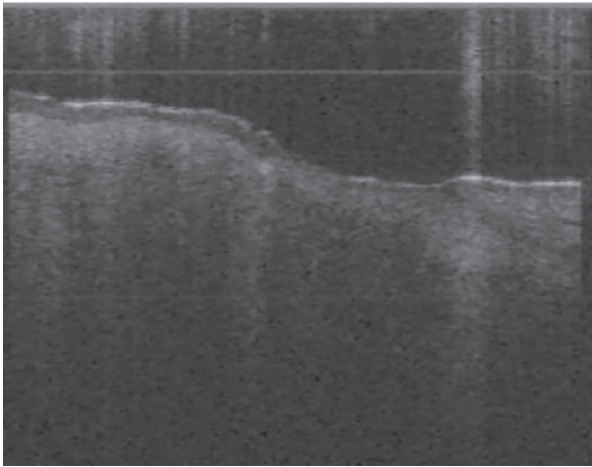*The OCT image of the benign melanocytic nevi.*

Figure 3.
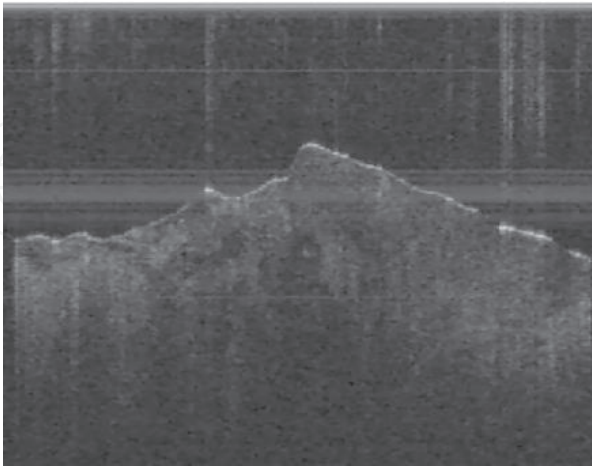*The OCT image of the basal cell carcinoma.*

Figure 4.
The OCT image of the melanoma.

without pigment are under the epidermis. Due to the heterogeneity of tumor, the randomly located multiform objects that have the different optical density can be visualized in the OCT images compared to the normal layered structure. The OCT image showed the dark or bright areas since the melanoma cells may have a surplus amount of pigment or may contain the nonpigmented elements.

OCT images were exported from the custom-built OCT system in the form of 8 bit gray level. The structural information of biological tissues can be recorded in OCT images. However, the OCT images contained not only the "useful" information but also the noise. A typical type of noise is called as "speckle" noise. The speckle noise is due to the limited spatial-frequency bandwidth of the interference signals in OCT [18]. Because OCT images were generated from OCT imaging system with the coherent detection, the speckle noise significantly blurred the contrast of OCT images by generating a grainy element in OCT images, which makes it harder to extract the features from OCT images. Therefore, it is necessary to remove the speckle noise from OCT images and then extract the FD to quantitatively classify the skin tumors. In this paper, the interval type II fuzzy anisotropic diffusion filter was employed to remove the speckle noise from OCT images [19].

2.3 Fractal analysis

In Euclidean space, structures consist of basic Euclidean geometries including lines, planes, and cubes. A straight line has exactly one dimension, a plane has exactly two dimensions, and a cube has exactly three dimensions. These basic shapes in integer dimensions were called "topological dimensions." For example, a fractal curve has dimensions between a straight line and a plane (between one and two), and a fractal surface has dimensions between a plane and a cube (between two and three). In order to determine the FD of complex objects, several definitions of FD were used. One simple and easily understandable definition of the FD is the Hausdorff dimension, which can be defined as follows:

$$FD = \lim_{r \to 0} \frac{\log N_r}{\log\left(\frac{1}{r}\right)}, \tag{1}$$

where N_r is the number of sets of cells (i.e., a ruler used to measure the coastline) and $1/r$ is the magnification factor that was used to reduce the cell in each spatial direction.

A typical example of a geometric object with a non-integer dimension is the Koch curve (see **Figure 5**). The straight line A, called the initiator, has a length of 1. The middle third of the line A was replaced with two lines that each line has the same length (1/3) as the remaining lines on each side. Thus, the length of the line B has a length 4/3. This form specifies a rule that is used to generate other new forms. Thus, the curve A was used as the initiator, and the curve B was used as generator for constructing the Koch curve. Each line was replaced with four lines, each 1/3 the length of the original. Therefore, the lengths of the lines C, D, and E are 16/9, 64/27, and 256/81, respectively. As indicated in **Figure 5**, the total length of the curve increases with each step, which leads to an infinite length. By applying Eq. (1), the relationship between $\log N_r$ and $\log(1/r)$ for the Koch curve, the FD could be calculated as $ln\,4/ln\,3 = 1.26$.

Moreover, the measurement of the FD of the coastline could be treated as the Koch curve, which naturally leads to the introduction of the box counting method. In the measurement of the coastline, the number of scaled ruler is also counted as and is the size of the cell (i.e., ruler). Equation (1) is used in the calculation of the FD. Note that the typical cell is a box-shaped cell (a square) for two-dimensional objects and that the typical cell is a cube for three-dimensional objects. The box counting method is considered the most accepted methodology to measure the FD in various applications due to its simplicity and automatic computability [20]. However, the box counting method was pointed to overcount or undercount the number of boxes (cells), which then led to an inaccurate calculation of the
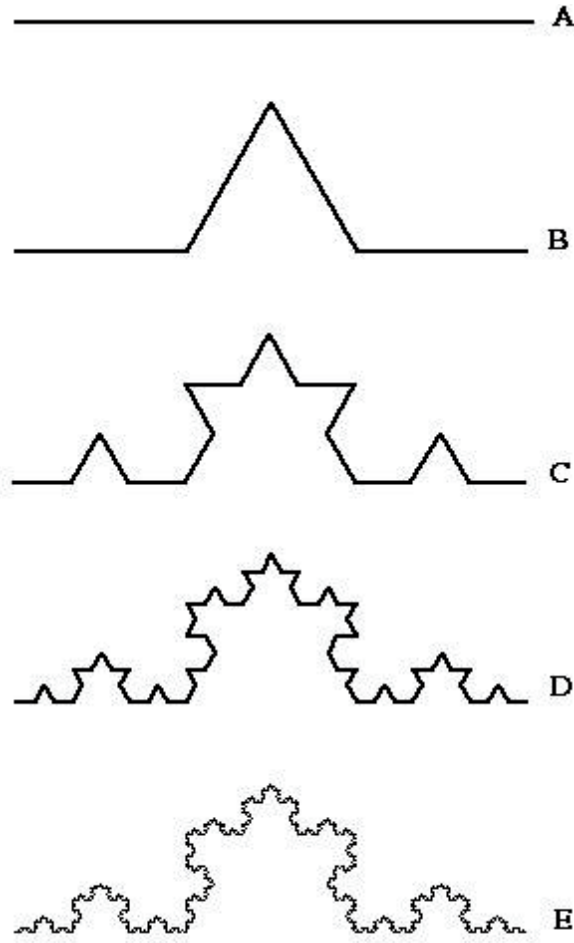
Figure 5.
Koch curve. The initiator (A) and generator (B) are used for constructing the Koch curve. Curves C, D, and E are levels 2, 3, and 4 in the construction of the Koch curve, respectively.

FD. Therefore, a more accurate and robust methodology, the 2D FAA, is utilized for the calculation of the FD.

The method for the calculation of the 2D Fourier FD is applied to a 2D grayscale image $I(k,l)$ with the size $N \times N$. The Fourier transform $\bar{I}$ can be expressed as follows:

$$\bar{I}(u,v) = \sum_{k=0}^{N-1}\sum_{l=0}^{N-1} I(k,l) \exp\left[-\frac{i2\pi}{N}(uk + vl)\right], \qquad (2)$$

where u and v are the horizontal and vertical frequency, respectively. The total frequency f is given by $f = \sqrt{u^2 + v^2}$. Then, the power spectrum of the 2D grayscale image $I(i,j)$ is given by

$$P = cf^{-\beta}, \qquad (3)$$

where c is a constant.

β can be calculated by fitting the function in Eq. (3) by calculating the slope of the curve $lnP \times lnf$. The least square method was used to obtain the slope in this paper. The 2D Fourier FD was then calculated by using the following equation [21]:

$$FD = \frac{8 - \beta}{2}. \qquad (4)$$

The range of possible values is between 2 and 3.

Another methodology the 2D DBCM will be used in this paper to calculate the FD. The detail of the 2D DBCM was introduced in Sarkar's paper [22].

3. Results and discussion

In our previous paper, the quantitative image features including the FD have already been studied to differentiate the skin tumors. However, the FD was extracted from OCT images by using the 2D DBCM. Generally speaking, the 2D DBCM is a time-consuming methodology. In order to quickly detect and classify the skin tumors, the 2D FAA was introduced in this paper. Twenty OCT images per type of skin tumors were randomly chosen from the database. The 2D FAA as well as the 2D DBCM was used to calculate the 2D FD. The FD calculated by using the 2D FAA and the statistical analysis between study groups were showed in **Table 1**. The FD that was obtained by employing the 2D DBCM and the statistical analysis between study groups were showed in **Table 2**. The averaged time for extracting the FD by using the two methodologies was showed in **Table 3**. The results in **Table 1** indicated that the Fourier FD of the basal cell carcinomas is significantly smaller than FD of melanomas. Compared to the FD value of melanomas, the Fourier FD of the basal cell carcinomas has a 2.79% decrease. The results also indicated that the Fourier FD of the benign melanocytic nevi is significantly smaller than FD of melanomas. Compared to the FD value of melanomas, the Fourier FD of the benign melanocytic nevi has a 2.69% decrease. The results in **Table 2** indicated that the FD of the basal cell carcinomas by using the 2D DBCM is significantly smaller than the FD of melanomas. Compared to the melanomas, the DBCM FD of the basal cell carcinomas has a 1.76% decrease. Compared to the melanomas, the DBCM FD of the benign melanocytic nevi showed the same tread. Specifically, the FD (calculated by using the 2D DBCM) of the benign melanocytic nevi decreased 1.38% as compared to the melanomas. In order to compare the computational time between the two methods, we run the two MATLAB codes (ver. R2007b) in the same laptop (i5-4210 CPU, 8GB RAM). In **Table 3**, the computational time was shorter by 91.71% for FAA than 2D DBCM.

Our results showed that the melanomas had a larger FD than the basal cell carcinomas and the benign melanocytic nevi when both of the two methodologies were utilized in the calculations. As the FD is used to express the abnormality of the biological tissue, our results suggested that the melanomas had more irregularity than the basal cell carcinomas and the benign melanocytic nevi. Melanomas feature heavily disorganized vessels with chaotic branching, which might be the explanation for that finding. These specific results indicated that both the Fourier FD and the differential box counting dimension could be used as an indicator to differentiate the melanomas from the basal cell carcinomas and the benign melanocytic nevi. It is worth noting that the Fourier FD is bigger than the differential box counting dimension in our calculations. The Fourier FD was calculated in the frequency domain, while the differential box counting dimension was calculated in the spatial domain. One possible reason to explain the difference is due to the undercount of the number of the boxes in the 2D DBCM which resulted in a small differential box counting dimension in the calculations. Moreover, our results also

Fractal analysis	Melanomas	Basal cell carcinomas	Nevi
FD	2.836 ± 0.031	2.757 ± 0.023[b]	2.760 ± 0.045[b]

[b]*p < 0:001 (ANOVA followed by Newman-Keuls post hoc analysis) between melanomas and benign melanocytic nevi (see nevi column) and between melanomas and basal cell carcinomas (see basal column)*

Table 1.
Distribution of FD (mean ± SD) values calculated by performing the FAA.

Fractal analysis	Melanomas	Basal cell carcinomas	Nevi
FD	2.388 ± 0.011	2.346 ± 0.013[b]	2.355 ± 0.008[b]

[b]$p < 0:001$ *(ANOVA followed by Newman-Keuls post hoc analysis) between melanomas and benign melanocytic nevi (see nevi column) and between melanomas and basal cell carcinomas (see basal column)*

Table 2.
Distribution of FD (mean ± SD) values calculated by using the DBCM.

	Fourier[1]	DBC[2]
Time(s)	0.088 ± 0.003	1.059 ± 0.020

[1]*Fourier: the 2D FAA*
[2]*DBC: the 2D DBCM*

Table 3.
Comparison of the computational time for calculating the FD by using the two methods.

showed that the differences of the Fourier FDs between the melanomas and the basal cell carcinomas are bigger than the differences of the differential box counting dimension, which could lead to a conclusion that the 2D Fourier FD could be better to classify the melanomas from the basal cell carcinomas. Our results also showed that the computational time for calculating 2D Fourier FD is much less than the computational time for calculating the 2D differential box counting dimension. This particular result suggested that the 2D FAA is more efficient to differentiate the skin tumors than the 2D DBCM.

There are several potential shortcomings of our study. The custom-built SD-OCT technology has some limitations as compared to the more pioneering OCT technology. In addition, current OCT devices include different algorithms and methodologies for the removal of the speckle noise. Therefore, data analysis is influenced by special assumptions and technological specifications that are in place for each individual OCT device. Another limitation is that only 20 scans were randomly selected for each type of skin tumors. Thus, more scans would be beneficial for extracting the more accurate FD and find the diagnostic parameter to differentiate the skin tumors.

4. Conclusion

In summary, we have described an efficient approach to calculate the 2D FD form OCT images for classifying the basal cell carcinomas, melanomas, and benign melanocytic nevi in this paper. The preliminary results presented have indicated that the 2D FAA is more efficient for extracting the FD than the 2D DBCM. Particularly, the change in the fractal dimension may reflect the pathological metabolic changes in melanomas. More research studies are needed to determine the accuracy, repeatability, and full capability of this methodology with more OCT images.

Acknowledgements

Author details

Wei Gao[1], Bingjiang Lin[2*], Valery P. Zakharov[3] and Oleg O. Myakinin[3]

1 School of Safety Engineering, Ningbo University of Technology, Ningbo, China

2 Ningbo First Hospital, Ningbo, China

3 Department of Laser and Biotechnical Systems, Samara National Research University, Samara, Russian Federation

*Address all correspondence to: bingjianglin@foxmail.com

IntechOpen

Gupta PK. Binary tissue classification studies on resected human breast tissues using optical coherence tomography images. Journal of Innovative Optical Health Sciences. 2011;**4**(1):59-66. DOI: 10.1142/S1793545811001083

[14] Mandelbrog BB. How long is the coast of Britian? Statistical self-similarity and fractal dimension. Science. 1967;**156**:636-638. DOI: 10.1126/science.156.3775.636

[15] Hussain RJ, Deviha VS, Rengarajan P. Analysing the invasiveness of skin cancer using fractals. International Journal of Engineering Research and Applications. 2012;**2**:2068-2075

[16] Karimi T, Farshchi SMR. Skin cancer expert system using fractal dimension. Research Journal of Pure Algebra. 2012;**2**:88-97

[17] Gao W, Zakharov VP, Myakinin OO, Bratchenko IA, Artemyev DN, Kornilin DV. Medical images classification for skin cancer using quantitative image features with optical coherence tomography. Journal of Innovative Optical Health Sciences. 2016;**9**(2):1650003. DOI: 10.1142/S1793545816500036

[18] Salinas HM, Fernandez DC. Comparison of PDE-based nonlinear diffusion approaches for image enhancement and denoising in optical coherence tomography. IEEE Transactions on Medical Imaging. 2007;**26**:761-771. DOI: 10.1109/TMI.2006.887375

[19] Puvanathasan P, Bizheva K. Interval type-II fuzzy anisotropic diffusion algorithm for speckle noise reduction in optical coherence tomography images. Optical Express. 2009;**17**:733-746. DOI: 10.1364/OE.17.000733

[20] Long M, Peng F. A box-counting method with adaptable box height for measuring the fractal feature of images. Radioengineering. 2013;**22**:208-213

[21] Ahammer H. Higuchi dimension of digital images. PLoS ONE. 2011;**6**:e24796. DOI: 10.1371/journal.pone.0024796

[22] Sarkar N, Chaudhuri BB. An efficient approach to estimate fractal dimension of textural images. Pattern Recognition. 1992;**25**:1035-1041. DOI: 10.1016/0031-3203(92)90066-r